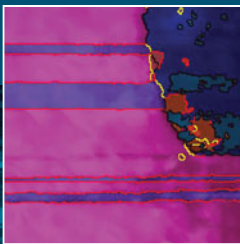

Synthesis and microstructure of electrodeposited and sputtered nanotwinned face-centered-cubic metals

Daniel C. Bufford, Y. Morris Wang, Yue Liu, and Lei Lu

The remarkable properties of nanotwinned (NT) face-centered-cubic (fcc) metals arise directly from twin boundaries, the structures of which can be initially determined by growth twinning during the deposition process. Understanding the synthesis process and its relation to the resulting microstructure, and ultimately to material properties, is key to understanding and utilizing these materials. This article presents recent studies on electrodeposition and sputtering methods that produce a high density of nanoscale growth twins in fcc metals. Nanoscale growth twins tend to form spontaneously in monolithic and alloyed fcc metals with lower stacking-fault energies, while engineered approaches are necessary for fcc metals with higher stacking-fault energies. Growth defects and other microstructural features that influence nanotwin behavior and stability are introduced here, and future challenges in fabricating NT materials are highlighted.

Introduction

Nanotwinned (NT) metals are a class of metallic materials with microstructures dominated by twin boundaries (TBs) spaced less than 100 nm. Compared to conventional grain boundaries (GBs), TBs have higher symmetry and lower energy, sometimes resulting in unique behaviors. NT metals show high strength while preserving ductility,[1–4] good work-hardening ability,[5] good electrical conductivity,[2,6] and improved resistance to electromigration[7] and corrosion.[8] These properties arise directly from the properties of TBs, and are distinct from those of nanocrystalline metals[9] (grain size <100 nm) of similar composition, but with high densities of conventional GBs. Such properties have drawn interest for the potential improvements they may provide to materials used in microelectronics[10] and microelectromechanical systems, while incorporation of these microstructures and properties in bulk structural materials remains a tantalizing possibility.

NT face-centered-cubic (fcc) metals have been extensively studied to date, as twins often form in these materials during a variety of synthesis processes ("bottom-up" approaches), or by processing bulk material ("top-down" approaches). In this overview, we focus specifically on electrodeposition and sputtering—two bottom-up deposition techniques that have been utilized extensively to fabricate NT metals with sample thicknesses ranging from nanometers to millimeters. Deformation twins and annealing twins will not be discussed here, nor will twins in low-dimensional materials such as nanoparticles, nanowires, or nanopillars. We refer interested readers to articles reviewing deformation-induced twinning processes,[11,12] and to the articles by Liao et al. and Raabe et al. in this issue.

The combination of microstructural features, including twin spacing and orientation, grain size, and the presence of other types of GBs ultimately determines the properties of NT materials. As such, it is meaningful to survey some of the important details regarding the finer structure of TBs, namely defects found along twins in electrodeposited and sputtered NT metals.

Nanotwin formation during fcc metal synthesis

Twinned structures appear in many crystalline materials, with the twin density determined by intrinsic material properties,

Daniel C. Bufford, Radiation-Solid Interactions Department, Sandia National Laboratories, USA; dcbuffo@sandia.gov
Y. Morris Wang, Lawrence Livermore National Laboratory, USA; wang35@llnl.gov
Yue Liu, Materials Science and Technology Division, Los Alamos National Laboratory, USA; yueliu@lanl.gov
Lei Lu, Institute of Metal Research, Chinese Academy of Sciences, China; llu@imr.ac.cn
DOI: 10.1557/mrs.2016.62

© 2016 Materials Research Society

Table I. Summary of nanotwinned face-centered-cubic (fcc) metal parameters (ordered by increasing stacking-fault energy, γ_{sf}).

Metal	γ_{sf} (mJ/m^2)	Method	Deposition Rate (nm/s)	*d* (µm)	λ (nm)	Reference
Cu-Al	6–13	MS	0.9–4.1	0.04–0.1	2–10	16
330 steel	*	MS	0.5	0.03	4	17,18
Ni-Co	*	PED	–	0.03	<10	19
Ag	16	MS	1.5–6	0.1–0.3	7–42	20–22
Cu	45–78	PED	1.5–7.5	0.5	15–96	3,4,6
		DCED	5.7	3.0–18.6	38–73	23
		MS	0.2–2.0	0.2	4–35	24,25
Ni	128	PED	–	0.1–0.4	18	10
Al	120–165	MS	0.5	–	–	26
Pd	175–180	EBE	–	0.026–0.2	20–35**	27–29

The corresponding deposition rates and resulting microstructural features, grain size (*d*) and twin spacing (λ) are also included. Note: PED, pulsed electrodeposition; DCED, direct-current electrodeposition; MS, magnetron sputtering; EBE, electron-beam evaporation.
*There are no γ_{sf} data for 330 stainless steel and Ni-Co in the literature, but they are expected to be low (i.e., <50 mJ/m^2).
**Sporadically spaced twin bundles.

growth conditions, and deformation/thermal history. The twinning plane can often be visualized as a mirror. Consider for example, the Σ3{111} twin boundary in fcc metals. The {111} plane is the boundary plane, and one of every three lattice sites is shared. This twin, often called the coherent twin boundary (CTB), switches from the abcabcabc stacking of unfaulted {111} planes to abcabacba, where the second b is the twining plane. The boundary itself can also be seen as a stacking fault (when approached from either direction). Twins form most readily in materials with low to moderate stacking-fault energies, γ_{sf}* (i.e., ~tens of mJ/m^2), however, twins may appear in metals with higher γ_{sf} under certain conditions. **Table I** summarizes details of selected fcc metals that have been the focus of NT metals research. We first discuss synthesis methods that capitalize on spontaneous-growth twin formation in lower γ_{sf} metals, then move on to special cases in which twins form in higher γ_{sf} metals.

Electrodeposition

Electrodeposition techniques were first developed two centuries ago. In recent years, they have been found to be effective for introducing high-density nanoscale growth twins in metals with appropriately low (i.e., below approximately 100 mJ/m^2) γ_{sf},[5] such as Cu,[1,2,14] Cu alloys,[4] Ni,[8] and Ni alloys.[15] The species to be deposited are initially chemically dissolved in an electrolyte solution. An electrical potential is applied, and the metal is deposited onto an electrode by means of an electrochemical reaction. Some parameters that influence twin formation, such as γ_{sf}, are controlled by material selection. Others depend on deposition conditions, with the main controllable parameters being temperature, chemistry, and current characteristics of the deposition process.

The simplest case is direct-current electrodeposition (DCED), in which a constant current is applied, resulting in a mostly constant growth rate of the film. Here, after an initial nucleation step, growth processes favoring strong {111} textures dominate, and twins form randomly due to the low γ_{sf}. The typical microstructure of NT metals prepared by DCED is characterized by columnar grains filled with high-density nanoscale CTBs, most of which are perpendicular to the growth direction,[14] (see **Figure 1**a).

A variation to this technique is pulsed electrodeposition (PED),[16] in which the power is repeatedly switched on and off with respective time intervals t_{on} and t_{off}. During t_{on}, the high-current density induces a high transient deposition rate, and the deposition process momentarily halts during t_{off}. Each pulse thus provides new nucleation opportunities, decreasing the strength of the {111} growth texture, and the higher transient deposition rate increases twin density. In contrast to DCED foils, PED NT Cu samples often have {110}-preferred orientations, with CTBs parallel to the growth direction,[3] as shown in Figure 1b.

During electrodeposition, the nucleation and growth rates of twins can be engineered by controlling the deposition parameters, such as peak and average current density, deposition rate, and bath chemistry. Current density plays an important role in NT Cu deposition; increasing current density from 10 mA/cm^2 to 30 mA/cm^2 decreased the average grain size in NT Cu foils from ~10 µm to 4 µm, while the twin spacing remained in the range of 30–50 nm.[17] This is because with an increase in current density, overpotential of the cathode increases and grain refinement (i.e., reduction of grain size) occurs.

*It should be noted that γ_{sf} and twin-boundary energy, γ_{tb}, typically are correlated for a given material, and thus both are frequently used in discussions of the tendency to form twins. Often, γ_{sf} is approximately 2γ_{tb}.[13]

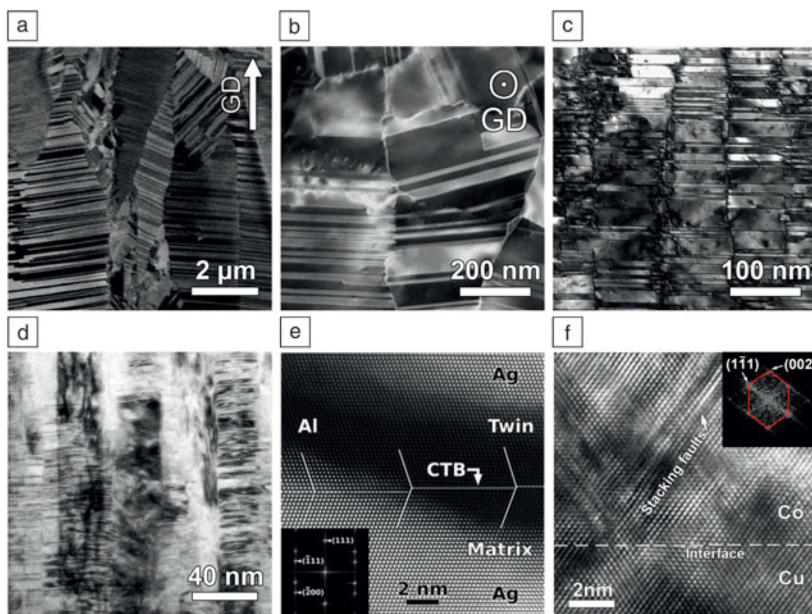

Figure 1. Transmission electron microscope micrographs (TEM) of nanotwinned (NT) microstructures resulting from different deposition methods and parameters. Note: GD, growth direction. (a) Columnar-grained polycrystalline NT Cu formed by direct-current electrodeposition.[14] (b) Equiaxed-polycrystalline NT Cu formed by pulsed electrodeposition.[3] (c) Sputtered columnar-grained polycrystalline NT Ag.[24] (d) Sputtered columnar-grained 330 stainless steel. Reproduced with permission from Reference 31. © 2005 American Institute of Physics. (e) Coherent-twin boundary (CTB) propagation across fully coherent interfaces in Ag/Al multilayer films.[32] (f) Inclined misfit stacking faults in Cu/Co multilayer films.

Effects of the average deposition rate on the twin density are also significant. Increasing the average deposition rate from 10 to 30 Å/s decreased the twin spacing from 90 nm to 15 nm in PED-deposited Cu foils, while further increasing the deposition rate to 80 Å/s achieved an average twin thickness as small as 4 nm.[1]

Different ions may be added to the electrolyte solution to influence various aspects of film growth, however, chloride (Cl^-) ions influence texture, particularly strongly in Cu.[18] With increasing chloride concentration in the electrolyte, DCED-deposited Cu films showed a monotonically strengthening {110} crystallographic texture, while PED films underwent a transition from {111} to {110} texture when chloride concentration decreased from 10^{-4} to 10^{-5} M.[19] The effect of chloride concentration on the crystallographic texture of the Cu films is attributed to differences in exchange current densities for different crystallographic planes.[19]

Varying amounts of bath components often end up in films during electrodeposition, including both those deliberately added to influence the deposition process and unanticipated impurities. These impurities may interfere with studies of the properties of twins in pure materials, or may cause undesirable behaviors such as embrittlement, however, there may be benefits to deliberately introduced chemical impurities. For example, certain impurities stabilize GBs at elevated temperatures[20] and may enhance thermal stability of twins.

Magnetron sputtering

In sputter deposition, a large potential accelerates ions from a plasma into the surface of the target material. These collisions eject atoms from the target, which travel across the vacuum chamber and condense on a substrate. The selected target material, substrate, and deposition parameters (including sputter power density, sputter gas pressure, substrate bias voltage, substrate temperature, and substrate-gun distance/orientation) control the film growth process.[21] As with electrodeposition techniques, dense TBs are often oriented perpendicular to the growth direction in metals with appropriately low γ_{sf}, for example, Cu,[22,23] Ag,[24–26] and alloy systems.[27–29] Different microstructures can be obtained from magnetron sputtering by changing substrates; columnar grains with strong {111} texture are common with fcc metals on most substrates,[30] however, NT microstructures with different orientations have been achieved by epitaxial growth.[24]

The tendency to spontaneously form growth twins has been explained by a thermodynamic vapor nucleation model in which the critical radii of formation for twinned and untwinned nuclei are considered.[28] According to this model, twin-boundary energy, γ_{tb}, and deposition rate are the two most important variables for controlling twin nucleation. Several studies have found qualitative agreement with this model, as NT microstructures appear frequently in low-γ_{tb} metals and alloys, such as Cu,[22] Ag (Figure 1c),[24] and 330 austenitic stainless steels (Figure 1d),[31] while metals with high γ_{tb} form twins sparsely under similar deposition conditions.[32] Also in agreement with the model, deposition rate was found to change twin density in Cu.[33]

In practice, film growth during magnetron sputtering is kinetically controlled, making the process difficult to fully describe by models derived from thermodynamics alone. Although the thermodynamic model discussed in the previous paragraph predicts that higher deposition rates should increase twin density, several experimental studies have indicated that this is not always the case.[26,34] In addition, the change in twin spacing is often accompanied by a change in grain size. These issues stem from the fact that adatom kinetic energy and flux affect the film growth process and twin-formation rates,[35] but these aspects are intrinsically tied to the same tunable sputtering parameters, making them difficult to control independently.[21,36] Additional systematic studies in both the experimental and modeling realms could refine the understanding of the influence of these deposition parameters on the twin-formation process.[37]

The sputtering process itself typically leaves only small amounts of incorporated sputter gas, but impurities may also originate in impure targets, surface contaminants (from targets

or substrates), or vacuum contaminants (e.g., oxygen, water vapor, and hydrocarbons). As with electrodeposition, it is desirable to minimize unwanted contaminants, however, deliberate inclusions may sometimes be useful, for example, to tailor γ_{sf} and hence to manipulate twin density[29] or as second-phase particles for additional hardening.[38]

In contrast to low-γ_{sf} metals, growth twins are rarely observed in high-γ_{sf} metals, such as Al, synthesized by either vapor- or electrodeposition.[32] However, fractions of growth twins were reported in nanocrystalline Pd prepared by electron-beam evaporation,[39] but not sputtering.[40] The nature of film growth during evaporation differs substantially from that of sputtering,[41] and results in a comparatively weaker {111} texture and lower-density twins with more random orientations than in other NT metals. The twin-formation mechanisms here are not yet completely understood. The unfavorable energetics of introducing twins spontaneously in high-γ_{sf} metals during deposition has led to the development of approaches using engineered microstructures, some of which will be discussed in the following paragraphs.

Recent studies have found mechanisms by which twins may form as a result of interfaces in a multilayer film structure. Interface coherency enables twin propagation from one layer to another, while in some multilayer films without coherent interfaces, misfit twins may form instead of dislocations to release the misfit strain. In multilayer film systems where the individual layer thickness, h, is small enough to maintain coherent growth, twins may propagate freely from one layer to the next,[32,42,43] as shown in Figure 1e.

Recent studies of other multilayer films without fully coherent interfaces suggest that layer-to-layer twin propagation can also occur between dissimilar planes, provided a point of local coherency along a twinning plane exists.[44] These studies suggest two criteria for formation of nanotwins by layer-to-layer propagation: (a) Twin nucleation in one layer, and (b) a coherent interface to ensure propagation. Mismatch or misfit twins refer to twins that form in only one layer to release misfit strain as an alternative to misfit dislocations. Such twins were first reported in semiconductors,[45] but have since been observed in several metallic systems,[46,47] including Cu/Co multilayer films, as shown in Figure 1f.[48] These twins typically appear only at semi-coherent interfaces (at large h), and propagate at an angle away from the interface.

Microstructure

Microstructural features, namely TBs, GBs, and certain defects, predominantly control the mechanical and physical properties in NT metals, so it is essential to discuss these microstructural details here in order to provide a full picture of the structure–property relationships in NT metals. We focus specifically on the microstructure, but we also direct the reader to the articles in this issue by Sansoz et al. and X. Li et al. for detailed discussions of the effects of these microstructural features on mechanical deformation.

Σ3 {111} and Σ3 {112} TBs

The two most commonly discussed TBs in fcc NT metals are Σ3{111} CTBs that appear as straight lines in transmission electron microscope (TEM) observations, and Σ3{112} incoherent TBs (ITBs) that can be identified by high-resolution TEM or inverse pole figure orientation mapping (IPFOM),[49] as shown in **Figure 2**a–b. CTBs have an ordered and symmetrical boundary structure, and typically exhibit much lower energy than conventional high-angle GBs; in Cu for example,

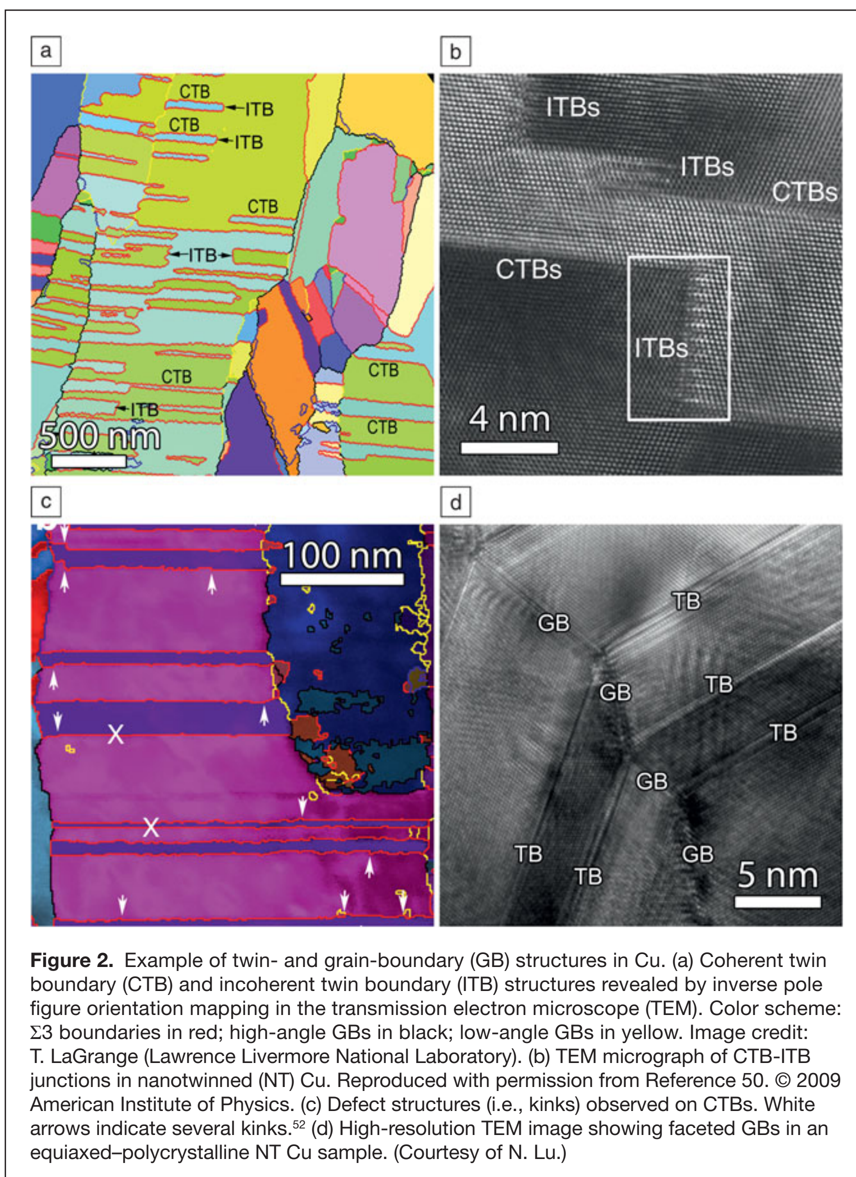

Figure 2. Example of twin- and grain-boundary (GB) structures in Cu. (a) Coherent twin boundary (CTB) and incoherent twin boundary (ITB) structures revealed by inverse pole figure orientation mapping in the transmission electron microscope (TEM). Color scheme: Σ3 boundaries in red; high-angle GBs in black; low-angle GBs in yellow. Image credit: T. LaGrange (Lawrence Livermore National Laboratory). (b) TEM micrograph of CTB-ITB junctions in nanotwinned (NT) Cu. Reproduced with permission from Reference 50. © 2009 American Institute of Physics. (c) Defect structures (i.e., kinks) observed on CTBs. White arrows indicate several kinks.[52] (d) High-resolution TEM image showing faceted GBs in an equiaxed–polycrystalline NT Cu sample. (Courtesy of N. Lu.)

CTBs, ITBs, and high-angle GBs have respective energies of 24–39 mJ/m^2, 590–714 mJ/m^2, and 625–710 mJ/m^2.[37,50] This has strong implications for both the thermal and mechanical stability of NT materials, as low-energy boundaries are often more resistant to migration processes.[4,37] CTBs are also known to scatter electrons less than GBs and thus help to maintain high electrical conductivity in NT metals.[6]

The Σ3{112} ITB structure can be described as three {111}⟨112⟩ partial dislocations occurring on three successive {111} planes, with the sum of their Burgers vectors = 0.[50,51] These dislocations may dissociate to a width determined by γ_{sf} and local stress to create a small volume of 9R phase (i.e., a periodically faulted structure with a stacking sequence of abcbcacab).[50] ITB energies tend to be closer to high-angle GB than CTB energies. In polycrystalline NT materials, ITBs mainly bound CTBs terminated inside grains (Figure 2a). However, subnanometer resolution IPFOM recently revealed that many as-grown CTBs contain ITBs that appear as steps along CTBs[52] (Figure 2c). The length of these ITBs in the ⟨111⟩ direction (perpendicular to the CTBs) is typically small (~2–5 nm), as seen in Figure 2c. The formation mechanisms of these ITBs along otherwise straight CTBs are poorly understood, but are expected to be linked to processing parameters. The existence of these defect structures along CTBs is consistent with the observations of partial dislocations impinged on CTBs in as-deposited material with twins spaced on the order of a few nm.[1]

Due to the low density of ITBs in typical NT metals, their influence on mechanical properties was initially thought to be inconsequential. However, the relatively high energy of ITBs leads to a tendency to migrate, where mobility is inversely proportional to the ITB length in the ⟨111⟩ direction.[52] It is clear from both simulations and experiments that these shorter ITBs are susceptible to migration under stresses, leading to annihilation of adjacent CTBs (i.e., detwinning).[51–54] ITBs may thus play critical roles in determining the maximum strength of NT metals,[1] and microstructure stability at elevated temperatures,[55] in radiation environments[56] and in fatigue-loading conditions.[57,58] However, it should be noted that longer ITBs are less mobile and may participate in strengthening and work hardening via dislocation interactions.[59,60] In light of these different behaviors, ITBs remain an active area of research interest, as it is clear that controlling ITB density is important for tailoring the overall material properties.

GBs in nanotwinned metals

The types of GBs in NT metals vary depending on the deposition procedure. GB orientation mapping of magnetron sputtered NT Cu in the TEM[52,54] suggested that the GB distribution in NT metals is far from the Mackenzie distribution of boundary misorientations, which is characteristic of a polycrystal with completely randomly oriented grains. This deviation indicates a strong preference for certain GBs, as opposed to a more random distribution. Epitaxial sputtered films[24,33] (Figure 1c and Figure 2b) may exhibit only ITBs in the growth direction, to the point that defining individual grains is difficult. In columnar-grained specimens obtained by electrodeposition or sputtering (Figure 1a and d), low-angle boundaries may join adjacent columns that are tilted or rotated with respect to the growth direction.[61]

A particularly interesting case is that of faceted GBs in PED Cu (Figure 2d). Here, GBs preferentially assume only a small number of low-energy crystallographic planes, and a high enough degree of faceting may lead to multifold twins.[62] The formation process for these GB-TB structures is not completely clear. It is possible that twinning and faceting reduce the total concentration of GB defects;[2,6] however, the associated high growth rate deposition processes are far from equilibrium, so energy minimization arguments are not fully satisfactory. Further work in unraveling the relationships between the growth process and these GBs is clearly needed.

GB-TB intersections may improve thermal stability by mutually pinning each other.[63,64] GBs are also considered to play important roles in mediating plasticity in NT metals.[14,52] Deformation anisotropy has been observed in highly textured NT materials,[65–67] as the ability of CTBs to block dislocation motion in the directions parallel and perpendicular to the boundary plane differs. As discussed earlier, CTBs have a strong tendency to align perpendicular to the growth direction in some deposition conditions, so a {111} texture is commonly observed in NT materials. There has been some success with PED and evaporation techniques in fabricating materials with more randomly oriented CTBs[1,14,39,40] or multifold twins;[62] such microstructures may contribute to less intense textures and more isotropic mechanical behavior.

Conclusion

NT metals have been fabricated by several deposition techniques, and a great variety of microstructures have been achieved by manipulating processing parameters. Further development of deposition techniques is needed to better tailor twin densities, grain sizes, and crystallographic texture to achieve desired properties. The vapor and electrochemical-based techniques presented here have practical upper thickness limits on the order of millimeter length scales, so producing thicker NT metals remains a challenging technical problem.

Extending the applicability of NT microstructures to other types of metals, especially those with high-γ_{sf} or non-fcc structures, is another challenge, while the properties of NT nonmetal systems remain largely unexplored. Interesting recent work has shown that dense stacking faults and twins in Mg alloys (with hexagonal close-packed structures)[68] and in diamond[69] contributed to novel properties. Such systems may provide rich environments for future work. Despite these challenges, synthesis and microstructural characterization of NT materials continue to offer many opportunities for both scientific materials research and engineering applications.

Acknowledgments

The authors thank N. Lu (Institute of Metals Research) and T. LaGrange (Lawrence Livermore National Laboratory) for

image contributions, and B.L Boyce, T.A. Furnish, K.M. Hattar, and B.R. Muntifering (Sandia National Laboratories) for helpful discussions. D.C.B. was fully supported by the Division of Materials Science and Engineering, Office of Basic Energy Sciences, US Department of Energy. Sandia National Laboratories is a multi-program laboratory managed and operated by Sandia Corporation, a wholly owned subsidiary of Lockheed Martin Corporation, for the US Department of Energy's National Nuclear Security Administration under Contract No. DE-AC04–94AL85000. The work on NT Al was supported by DoE-OBES under Grant No. DE-SC0010482. The work (Y.M.W.) at Lawrence Livermore National Laboratory was supported by the US Department of Energy under Contract DE-AC52–07NA27344. Y.L. was fully supported by the Office of Basic Energy Sciences, Project FWP 06SCPE401, under US DoE Contract No. W-7405-ENG-36. L.L. acknowledges financial support from the National Basic Research Program of China (973 Program, 2012CB932202), the NSFC (Grant Nos. 51420105001, 51371171, and 51471172) and the "Hundreds of Talents Project" from CAS.

References

1. L. Lu, X. Chen, X. Huang, K. Lu, *Science* **323**, 607 (2009).
2. L. Lu, Y.F. Shen, X.H. Chen, L.H. Qian, K. Lu, *Science* **304**, 422 (2004).
3. Y.F. Shen, L. Lu, Q.H. Lu, Z.H. Jin, K. Lu, *Scr. Mater.* **52**, 989 (2005).
4. K. Lu, L. Lu, S. Suresh, *Science* **324**, 349 (2009).
5. L. Lu, Z.S. You, K. Lu, *Scr. Mater.* **66**, 837 (2012).
6. X.H. Chen, L. Lu, K. Lu, *J. Appl. Phys.* **102**, 083708 (2007).
7. K.C. Chen, W.W. Wu, C.N. Liao, L.J. Chen, K.N. Tu, *Science* **321**, 1066 (2008).
8. G.Z. Meng, Y.W. Shao, T. Zhang, Y. Zhang, F.H. Wang, *Electrochim. Acta* **53**, 5923 (2008).
9. M.A. Meyers, A. Mishra, D.J. Benson, *Prog. Mater. Sci.* **51**, 427 (2006).
10. T.C. Liu, C.M. Liu, Y.S. Huang, C. Chen, K.N. Tu, *Scr. Mater.* **68**, 241 (2013).
11. J.W. Christian, S. Mahajan, *Prog. Mater. Sci.* **39**, 1 (1995).
12. Y.T. Zhu, X.Z. Liao, X.L. Wu, *Prog. Mater. Sci.* **57**, 1 (2012).
13. J.P. Hirth, J. Lothe, *Theory of Dislocations* (Krieger Publishing, Malabar, FL, 1982).
14. Z.S. You, L. Lu, K. Lu, *Acta Mater.* **59**, 6927 (2011).
15. B.Y.C. Wu, P.J. Ferreira, C.A. Schuh, *Metall. Mater. Trans. A* **36A**, 1927 (2005).
16. M.S. Chandrasekar, M. Pushpavanam, *Electrochim. Acta* **53**, 3313 (2008).
17. S. Jin, Q.S. Pan, L. Lu, *Acta Metall. Sin.* **49**, 635 (2013).
18. N. Vasiljevic, M. Wood, P.J. Heard, W. Schwarzacher, *J. Electrochem. Soc.* **157**, D193 (2010).
19. T.C. Chan, Y.L. Chueh, C.N. Liao, *Cryst. Growth Des.* **11**, 4970 (2011).
20. C.C. Koch, R.O. Scattergood, M. Saber, H. Kotan, *J. Mater. Res.* **28**, 1785 (2013).
21. M. Ohring, *Materials Science of Thin Films*, 2nd ed. (Academic Press, San Diego, 2001).
22. A.M. Hodge, Y.M. Wang, T.W. Barbee, *Mater. Sci. Eng. A* **429**, 272 (2006).
23. X. Zhang, H. Wang, X.H. Chen, L. Lu, K. Lu, R.G. Hoagland, A. Misra, *Appl. Phys. Lett.* **88**, 173116 (2006).
24. D. Bufford, H. Wang, X. Zhang, *Acta Mater.* **59**, 93 (2011).
25. T.A. Furnish, A.M. Hodge, *APL Mater.* **2**, 046112 (2014).
26. R.T. Ott, J. Geng, M.F. Besser, M.J. Kramer, Y.M. Wang, E.S. Park, R. LeSar, A.H. King, *Acta Mater.* **96**, 378 (2015).
27. X. Zhang, A. Misra, H. Wang, A.L. Lima, M.F. Hundley, R.G. Hoagland, *J. Appl. Phys.* **97**, 094302 (2005).
28. X. Zhang, A. Misra, H. Wang, T.D. Shen, M. Nastasi, T.E. Mitchell, J.P. Hirth, R.G. Hoagland, J.D. Embury, *Acta Mater.* **52**, 995 (2004).
29. L. Velasco, M.N. Polyakov, A.M. Hodge, *Scr. Mater.* **83**, 33 (2014).
30. A.M. Hodge, Y.M. Wang, T.W. Barbee, *Scr. Mater.* **59**, 163 (2008).
31. X. Zhang, A. Misra, H. Wang, J.G. Swadener, A.L. Lima, M.F. Hundley, R.G. Hoagland, *Appl. Phys. Lett.* **87**, 233116 (2005).
32. D. Bufford, Y. Liu, Y. Zhu, Z. Bi, Q.X. Jia, H. Wang, X. Zhang, *Mater. Res. Lett.* **1**, 51 (2013).
33. O. Anderoglu, A. Misra, H. Wang, F. Ronning, M.F. Hundley, X. Zhang, *Appl. Phys. Lett.* **93**, 083108 (2008).
34. X. Zhang, O. Anderoglu, A. Misra, H. Wang, *Appl. Phys. Lett.* **90**, 153101 (2007).
35. S.D. Dahlgren, W.L. Nicholson, M.D. Merz, W. Bollmann, J.F. Devlin, D.R. Wang, *Thin Solid Films* **40**, 345 (1977).
36. L.B. Freund, S. Suresh, *Thin Film Materials: Stress, Defect Formation and Surface Evolution* (Cambridge University Press, New York, 2009).
37. X. Zhang, O. Anderoglu, R.G. Hoagland, A. Misra, *JOM* **60**, 75 (2008).
38. H. Ma, Y. Zou, A.S. Sologubenko, R. Spolenak, *Acta Mater.* **98**, 17 (2015).
39. H. Idrissi, B.J. Wang, M.S. Colla, J.P. Raskin, D. Schryvers, T. Pardoen, *Adv. Mater.* **23**, 2119 (2011).
40. B. Wang, H. Idrissi, H. Shi, M.S. Colla, S. Michotte, J.P. Raskin, T. Pardoen, D. Schryvers, *Scr. Mater.* **66**, 866 (2012).
41. J.A. Thornton, *Annu. Rev. Mater. Sci.* **7**, 239 (1977).
42. Y. Liu, D. Bufford, H. Wang, C. Sun, X. Zhang, *Acta Mater.* **59**, 1924 (2011).
43. Y. Liu, D. Bufford, S. Rios, H. Wang, J. Chen, J.Y. Zhang, X. Zhang, *J. Appl. Phys.* **111**, 073526 (2012).
44. K.Y. Yu, D. Bufford, Y. Chen, Y. Liu, H. Wang, X. Zhang, *Appl. Phys. Lett.* **103**, 181903 (2013).
45. W. Wegscheider, K. Eberl, G. Abstreiter, H. Cerva, H. Oppolzer, *Appl. Phys. Lett.* **57**, 1496 (1990).
46. M. Dynna, A. Marty, B. Gilles, G. Patrat, *Acta Mater.* **45**, 257 (1997).
47. Y.S. Zhang, L.L. Liu, T.Y. Zhang, *J. Appl. Phys.* **101**, 063502 (2007).
48. Y. Liu, Y. Chen, K.Y. Yu, H. Wang, J. Chen, X. Zhang, *Int. J. Plast.* **49**, 152 (2013).
49. E. Rauch, M. Veron, J. Portillo, D. Bultreys, Y. Maniette, S. Nicolopoulos, *Microsc. Anal.* **128**, S5 (2008).
50. J. Wang, O. Anderoglu, J.P. Hirth, A. Misra, X. Zhang, *Appl. Phys. Lett.* **95**, 021908 (2009).
51. L. Xu, D. Xu, K.N. Tu, Y. Cai, N. Wang, P. Dixit, J.H.L. Pang, J.M. Miao, *J. Appl. Phys.* **104**, 113717 (2008).
52. Y.M. Wang, F. Sansoz, T. LaGrange, R.T. Ott, J. Marian, T.W. Barbee, A.V. Hamza, *Nat. Mater.* **12**, 697 (2013).
53. J. Wang, N. Li, O. Anderoglu, X. Zhang, A. Misra, J.Y. Huang, J.P. Hirth, *Acta Mater.* **58**, 2262 (2010).
54. T. LaGrange, B.W. Reed, M. Wall, J. Mason, T. Barbee, M. Kumar, *Appl. Phys. Lett.* **102**, 011905 (2013).
55. D. Bufford, H.Y. Wang, X.H. Zhang, *J. Mater. Res.* **28**, 1729 (2013).
56. Y. Chen, K.Y. Yu, Y. Liu, S. Shao, H. Wang, M.A. Kirk, J. Wang, X. Zhang, *Nat. Commun.* **6**, 7036 (2015).
57. C.J. Shute, B.D. Myers, S. Xie, S.Y. Li, T.W. Barbee, A.M. Hodge, J.R. Weertman, *Acta Mater.* **59**, 4569 (2011).
58. B.G. Yoo, S.T. Boles, Y. Liu, X. Zhang, R. Schwaiger, C. Eberl, O. Kraft, *Acta Mater.* **81**, 184 (2014).
59. N. Li, J. Wang, X. Zhang, A. Misra, *JOM* **63**, 62 (2011).
60. D. Bufford, Y. Liu, J. Wang, H. Wang, X. Zhang, *Nat. Commun.* **5**, 4864 (2014).
61. O. Anderoglu, A. Misra, H. Wang, X. Zhang, *J. Appl. Phys.* **103**, 094322 (2008).
62. Y. Zhang, J. Wang, H. Shan, K. Zhao, *Scr. Mater.* **108**, 35 (2015).
63. C. Saldana, T.G. Murthy, M.R. Shankar, E.A. Stach, S. Chandrasekar, *Appl. Phys. Lett.* **94**, 021910 (2009).
64. Y.F. Zhao, T.A. Furnish, M.E. Kassner, A.M. Hodge, *J. Mater. Res.* **27**, 3049 (2012).
65. J.C. Ye, Y.M. Wang, T.W. Barbee, A.V. Hamza, *Appl. Phys. Lett.* **100**, 261912 (2012).
66. Z.S. You, X.Y. Li, L.J. Gui, Q.H. Lu, T. Zhu, H.J. Gao, L. Lu, *Acta Mater.* **61**, 217 (2013).
67. D.C. Jang, X.Y. Li, H.J. Gao, J.R. Greer, *Nat. Nanotechnol.* **7**, 594 (2012).
68. W.W. Jian, G.M. Cheng, W.Z. Xu, H. Yuan, M.H. Tsai, Q.D. Wang, C.C. Koch, Y.T. Zhu, S.N. Mathaudhu, *Mater. Res. Lett.* **1**, 61 (2013).
69. Q. Huang, D.L. Yu, B. Xu, W.T. Hu, Y.M. Ma, Y.B. Wang, Z.S. Zhao, B. Wen, J.L. He, Z.Y. Liu, Y.J. Tian, *Nature* **510**, 250 (2014). □

Join or renew Today!
Your MRS Membership now includes online access to ALL MRS Publications.